Deep Learning Analysis of Vibrational Spectra of Bacterial Lysate for Rapid Antimicrobial Susceptibility Testing

William John Thrift, Sasha Ronaghi, Muntaha Samad, Hong Wei, Dean Gia Nguyen, Antony Superio Cabuslay, Chloe E. Groome, Peter Joseph Santiago, Pierre Baldi, Allon I. Hochbaum, and Regina Ragan*

ACCESS | Metrics & More | Article Recommendations | SI Supporting Information

ABSTRACT: Rapid antimicrobial susceptibility testing (AST) is an integral tool to mitigate the unnecessary use of powerful and broad-spectrum antibiotics that leads to the proliferation of multi-drug-resistant bacteria. Using a sensor platform composed of surface-enhanced Raman scattering (SERS) sensors with control of nanogap chemistry and machine learning algorithms for analysis of complex spectral data, bacteria metabolic profiles post antibiotic exposure are correlated with susceptibility. Deep neural network models are able to discriminate the responses of *Escherichia coli* and *Pseudomonas aeruginosa* to antibiotics from untreated cells in SERS data in 10 min after antibiotic exposure with greater than 99% accuracy. Deep learning analysis is also able to differentiate responses from untreated cells with antibiotic dosages up to 10-fold lower than the minimum inhibitory concentration observed in conventional growth assays. In addition, analysis of SERS data using a generative model, a variational autoencoder, identifies spectral features in the *P. aeruginosa* lysate data associated with antibiotic efficacy. From this insight, a combinatorial dataset of metabolites is selected to extend the latent space of the variational autoencoder. This culture-free dataset dramatically improves classification accuracy to select effective antibiotic treatment in 30 min. Unsupervised Bayesian Gaussian mixture analysis achieves 99.3% accuracy in discriminating between susceptible *versus* resistant to antibiotic cultures in SERS using the extended latent space. Discriminative and generative models rapidly provide high classification accuracy with small sets of labeled data, which enormously reduces the amount of time needed to validate phenotypic AST with conventional growth assays. Thus, this work outlines a promising approach toward practical rapid AST.

KEYWORDS: surface-enhanced Raman scattering, machine learning, deep neural networks, variational autoencoders, generative deep learning, antimicrobial susceptibility testing, antimicrobial resistance
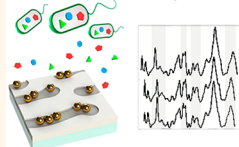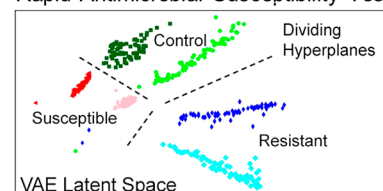
Worldwide, 700,000 people die annually of bacterial infections exhibiting antimicrobial resistance.[1] A full third of antibiotics prescribed are to treat bacteria that are resistant to those therapeutics, or which are otherwise inappropriate.[2] Antimicrobial resistance is a growing problem, and by 2050 it is expected to cause 10 million deaths per year and a 3.8% reduction of the total world gross domestic product.[3] While it is a multifaceted problem that will require many systemic changes to healthcare, the 2016 Review on Antimicrobial Resistance includes rapid diagnostics, referred to as antimicrobial susceptibility tests (AST), to reduce the unnecessary use of antimicrobials as a key intervention for the reduction of antimicrobial resistance.[4] Conventionally, AST involves acquiring clinical samples from patients, culturing the samples for 24−72 h,[5] and using disk-diffusion or broth microdilution assays (among other techniques) to identify a suitable antibiotic for treatment,[6] which does reduce hospital stays and save money despite long culture times.[10] Yet AST results are required within a typical doctor visit for reducing inappropriate use of antibiotics to mitigate antimicrobial resistance proliferation while maintaining optimal patient
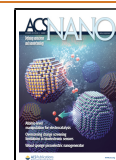
outcomes.[7−9] Point-of-care genomic AST, using genetic markers (genes, plasmids, or mutations) associated with resistance, potentially obviates the need for culturing and has shown promising results on the time scale of hours. Yet the presence of resistance genes does not necessarily translate to expressed (phenotypic) resistance.[10,11] Furthermore, genotypic AST detects only known genes and mutations associated with resistance, and does not allow for guarding against emergence of recently evolved resistance mechanisms. For these reasons, phenotypic AST is considered the gold standard,[12] and often genomic AST still requires phenotypic validation.[13−15]

Here we present a nanosensor platform for phenotypic AST using bacterial metabolite profiles post antibiotic exposure and correlating with antibiotic susceptibility. Metabolomic analyses of the bacterial response to antibiotic treatment, using standard methods such as mass spectrometry,[16−19] show that the mechanism of killing of antibiotics generally depends on the dysregulation of core metabolic function,[20−23] and substantial, yet similar, changes in metabolite profiles of *E. coli* were observed within 30 min after treatment with three classes of antibiotics: β-lactams, aminoglycosides, and quinolones.[20] Surface-enhanced Raman scattering (SERS) spectroscopy is a low-cost alternative to mass spectroscopy able to differentiate complex mixtures of small molecules with a label-free approach[24−27] and detect concentrations as low as 1 part per trillion.[31] Advanced nanomanufacturing methods, such as the two-dimensional physically activated chemical (2PAC) assembly method we previously developed,[28,29] permit the rapid acquisition of large datasets from SERS substrates with controlled plasmonic nanogaps due to their high sensitivity and consequently short exposure times necessary to acquire reproducible spectra.[30,31] 2PAC-fabricated sensors are capable of measuring single-molecule detection events and, with a machine learning approach, able to quantify molecular concentration down to 10 fM.[30] SERS has been extensively used in bacterial detection,[32−34] and metabolites identified with SERS[35] have been validated by mass spectroscopy.[36] Differential changes in vibrational peak intensity in SERS spectra without recognition molecules have been correlated with antimicrobial susceptibility, with minimum inhibitory concentrations of antibiotics in 1 h after antibiotic exposure,[37] and with susceptibility to antibiotics in 2 h in microfluidic channels.[38]

Yet, in order for SERS-based AST to enter general use in healthcare, spectral analysis must be robust enough to capture the diversity and complexity of the bacterial systems observed in a clinical setting, *i.e.*, with methods that go beyond specific peak intensities. Machine learning, especially deep learning,[39−42] is emerging as an important force to revolutionize healthcare, with these approaches now surpassing the performance of doctors in computer vision tasks like diagnosing skin,[43] breast,[44,45] and other forms of cancer.[46−48] Raman + deep learning has shown promise for AST and reports that analysis can benefit from enhancements in SERS but requires an approach to overcome lack of reproducibility in SERS data.[49] Since the use of principal component analysis to demonstrate single-molecule detection by Le Ru et al.,[50] great progress has been made in applying sophisticated machine learning techniques to analyze SERS spectra. These include fully connected artificial neural networks for analyte concentration regression,[51] DNA classification,[52] cancer detection,[53] convolutional neural networks for classification of metabolite signals,[26] support vector machines for classification of drug use from urine,[54] and genetic algorithms for cancer diagnoses.[55] From this discussion, it seems like a deep learning based SERS approach to AST would be easily implemented due to the practicality of collecting large SERS datasets of bacterial metabolites. Yet, in addition to the challenge of fabricating SERS sensors with reproducible response,[26,49,56−58] rapid AST sensor data must be validated with traditional AST approaches to be accepted into practical use.[12,59] This means that every antimicrobial resistance status label that corresponds to a SERS spectrum will require a 24−72 h culturing process. Considering that deep learning algorithms that tackle healthcare problems may require thousands of labeled examples,[60] this timeline represents an enormous barrier for the development of SERS AST in a clinical setting.

In this work, we apply deep learning methods, which have shown promise for healthcare,[61,62] to greatly reduce the amount of labeled data needed for high classification accuracy in differentiating bacterial metabolite profiles from SERS data. SERS analysis of cell lysate from *Pseudomonas aeruginosa* and *Escherichia coli* after different antibiotic treatments shows differential responses when using unsupervised variational autoencoder methods to derive compact representations of the data and deep feedforward discriminative networks to analyze both the dose and temporal responses and derive useful predictors.[54] Deep neural network discriminative models are able to differentiate metabolic response from treated and untreated bacteria with greater than 99% accuracy as early as 10 min for both *E. coli* and *P. aeruginosa*. Similarly, for the dosage-varied data, these discriminative models are able to differentiate treated from untreated bacteria with a very high accuracy with concentrations as low as 0.1 μg/mL. Conventional growth assays do not exhibit differential responses in cell density with respect to untreated cells at this antibiotic dose. Furthermore, this observed differentiation in the models is observed when they are exposed to antibiotic concentrations 10-fold lower than prior reported values of the minimum inhibitory concentration for both pathogens. Deep learning methods are then extended to investigate *P. aeruginosa* that has been treated with different antibiotics of varying efficacy. The generative nature of a variational autoencoder is used to identify the vibrational regions that collectively demonstrate the greatest change between antibiotic resistant, susceptible, and untreated SERS spectra in the AST dataset. Training algorithms with 63 targeted mixtures of bacterial metabolites in vibrational regions of interest greatly improve clustering of SERS AST spectra without any increase of labeled (cell culture) data. We refer to this as *data-informed transfer learning*, where the metabolite mixtures for further training have vibrational features in the frequency range to improve downstream model performance. Data-informed transfer learning achieves greater than 98% accuracy when analyzed with two different approaches: an unsupervised Bayesian Gaussian mixture model and a deep convolutional neural network model, with fewer than 10 examples, *i.e.*, 10 spectra from each class. This work is an important proof of concept, demonstrating that deep learning analysis of SERS data provides a rapid method for clinical AST.

RESULTS AND DISCUSSION

In order to reduce the time required for phenotypic AST, we pursue a metabolomics approach rather than direct measurement of cell growth or viability, as recent studies on metabolite responses to antibiotic exposure indicate that a rapid metabolic
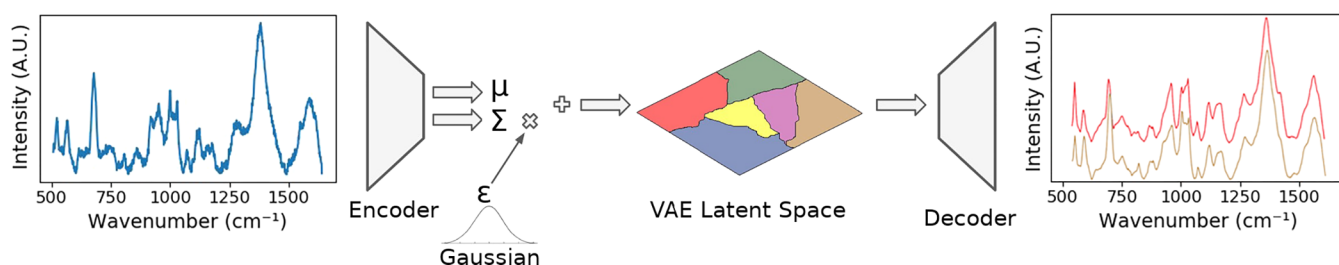
Figure 1. (Left) Example of SERS training spectrum. (Center) Depiction of the VAE model where spectra are encoded into the latent space as Gaussian distributions with mean μ and variance Σ. The encoder and decoder models are deep convolutional neural networks. (Right) The spectrum shown on the left is encoded, decoded, and plotted as the brown curve. The red curve overlaid here highlights differences in spectra in clusters in VAE space.
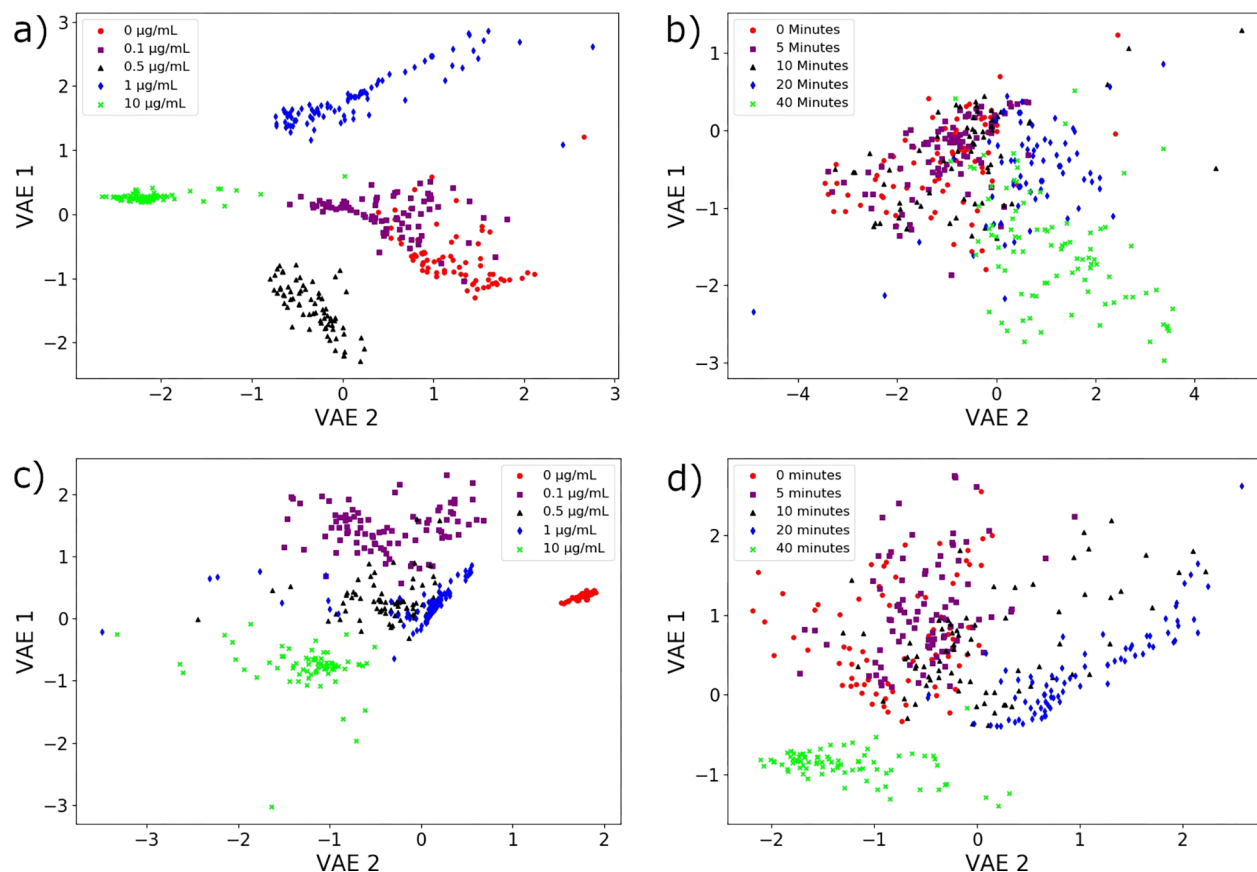

Figure 2. (a, c) VAE latent space depicting analysis of SERS spectra of dose response of *P. aeruginosa* (a) and *E. coli* (c) where analysis of 0, 0.1, 0.5, 1, and 10 μg/mL gentamicin dosed lysate are depicted in red, purple, black, blue, and green, respectively. b, d) VAE latent spaces of temporal response of *P. aeruginosa* (b) and *E. coli* (d) where lysate processed after 0, 5, 10, 20, and 40 min of 10 μg/mL gentamicin dosage are depicted in red, purple, black, blue, and green, respectively.

profiling technique is able to detect phenotypic susceptibility or resistance to antibiotics.[20−23,63] Yet, there is an important price to pay to reduce AST time in this way: metabolomics approaches introduce an enormous parameter space. Consider that the *E. coli* metabolome contains over 2600 different metabolites.[64] Nevertheless, SERS spectroscopy is an ideal method to address this issue due to the speed and simplicity of sample preparation of, for example, 2PAC sensor surfaces.[29,31] When complemented with machine learning analysis, the rich vibrational information from 2PAC sensors has been used to detect and monitor bacterial biofilm formation before some adapted antimicrobial resistance mechanisms are activated.[34] While a deep learning approach is essential, when building models that capture the complexity of SERS spectra of

bacterial metabolites it is important to determine how to optimize prediction accuracy with deep neural network models while minimizing the amount of cell culture data needed for training. We use feed-forward deep neural network models to differentiate the treatment conditions with near perfect accuracy in tandem with deep generative models, *i.e.*, the variational autoencoder, that give the user insight into the model's decision-making.

Development of Deep Neural Network Models for Antimicrobial Susceptibility Testing. Figure 1 depicts the scheme for using a variational autoencoder (VAE) for SERS analysis. The VAE works by encoding a high-dimensional data point (here, a SERS spectrum) into a low-dimensional latent space to capture an essential representation of the data. The
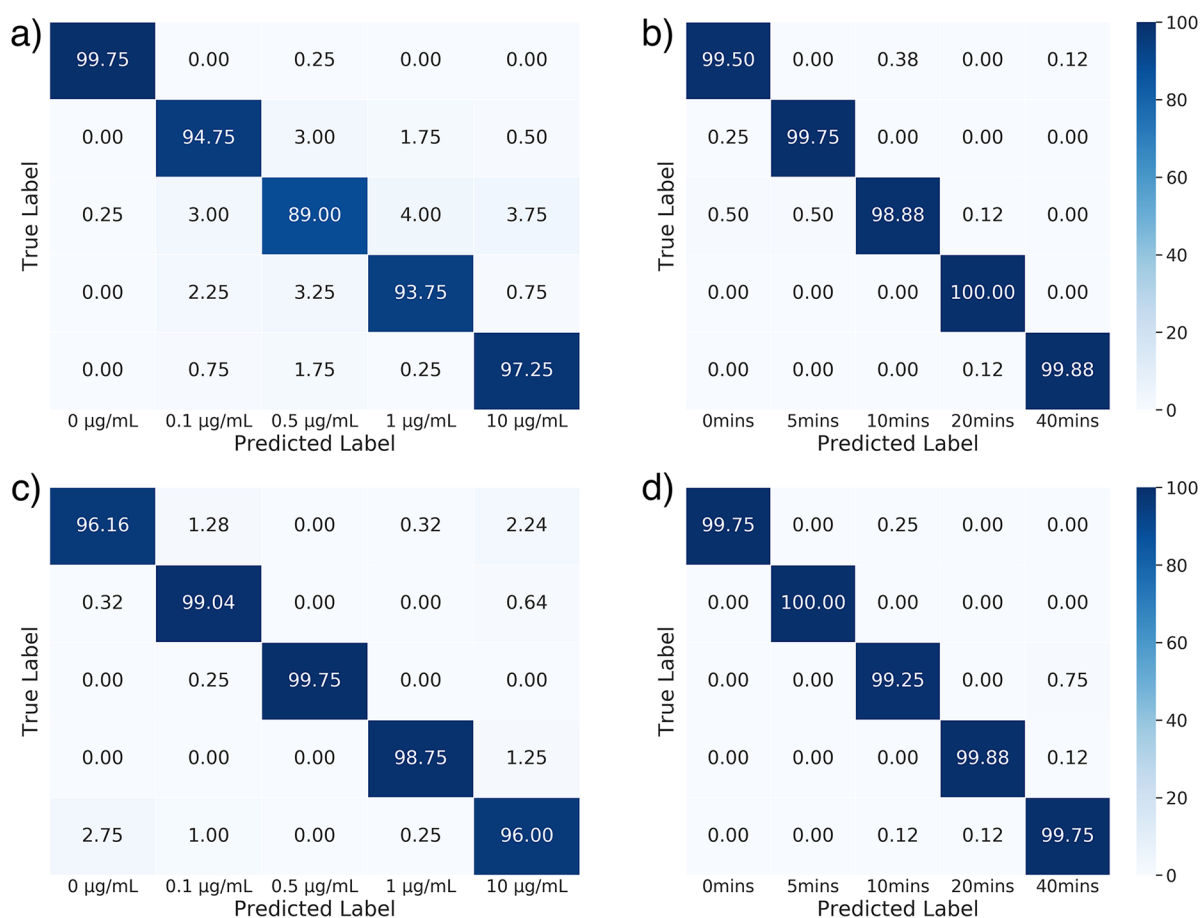
Figure 3. Five-class DNN model confusion matrices (values are listed as percentages). The datasets used are *E. coli* (a) gentamicin dose and (b) temporal response dataset, and *P. aeruginosa* (c) gentamicin dose and (d) temporal response dataset.

VAE is composed of an encoder network that encodes spectra as a Gaussian probability distribution in the *n*-dimensional latent space, schematically depicted as μ and Σ, and a decoder network that samples points from the latent space and decodes them back into the original spectra. The construction of our VAE using deep convolutional neural networks, architecture, and training parameters is further described in the Methods.

By encoding spectra as probability distributions in a lower dimensional latent space, the VAE provides us with three useful features: (1) Clustering—as all spectra are encoded as distributions, they will overlap with one another. If overlapping distributions are not from similar spectra, the model will be heavily penalized during training. This results in a well structured latent space that enables the use of simple models to make predictions from encoded data. (2) De-noising—the low-dimensional latent space does not contain enough information to encode for noise. This improves predictions made from models trained on encoded data, especially for small amounts of labeled data. (3) Interpretation—encoding spectra as distributions ensures that the latent space will be a continuous representation of the different classes of antibiotic treatments. This allows us to decode spectra and visualize variations across the latent space to ensure decoded spectra represents experimental data and identify vibrational features associated with susceptibility *versus* resistance.

The VAE latent space enables supervised classification techniques for clustering of SERS spectra of bacterial lysates exposed to various antibiotic conditions. The bacterial response was also characterized with traditional growth assays to define the minimum inhibitory concentration of antibiotic which inhibits 50% of growth at control conditions (MIC_{50}) as the MIC is strongly dependent on cell growth conditions.[65] Prior to training the VAE, SERS spectra are pre-processed as described in the Methods. We first demonstrate VAE performance for visually differentiating spectra from *E. coli* and *P. aeruginosa* lysate as a function of time and dosage. Bacterial cultures were prepared as described in the Methods and re-suspended before treatment in fresh lysogeny broth (LB) to an optical density at 600 nm (OD_{600}) of 0.5. Encoded SERS spectra from cellular lysate with varying dose and temporal response of *P. aeruginosa* and *E. coli* when exposed to gentamicin are plotted in Figure 2. For the dosage data, cells were processed 30 min post antibiotic exposure. Spectra are encoded using a VAE trained with the spectral dataset from bacterial lysate at experimental conditions indicated for each panel. While these plots are arbitrarily rotated about VAE axes, differences in the relative location of data within VAE latent space represent corresponding changes of features within the spectra. Thus, it is notable that the largest difference in VAE values, with respect to untreated conditions, are observed in spectral lysate data above the MIC_{50}, demonstrating that this approach provides a gradient of phenotypic feedback. When analyzing the SERS spectra from these bacteria using the VAE method, one can begin to observe differentiation of *P. aeruginosa* and *E. coli* lysate data in Figure 2a,c at concentrations as low as 0.1 μg/mL, an order of magnitude
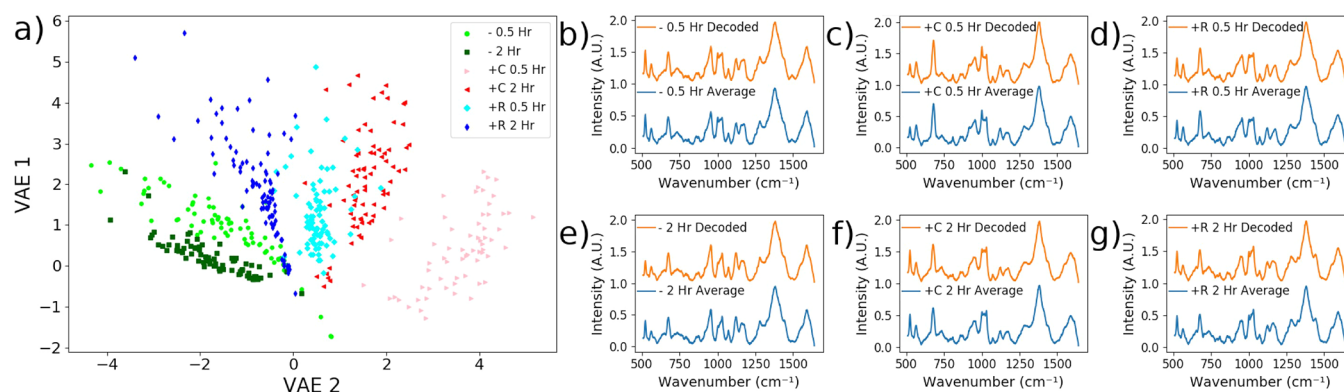
Figure 4. (a) VAE space of AST spectra from untreated [−]*P. aeruginosa* lysate (0.5 h/2 h, light/dark green), 50 μg/mL carbenicillin-treated [+C] *P. aeruginosa* lysate (0.5 h/2 h, light/dark red), and 400 μg/mL rifampicin-treated [+R] *P. aeruginosa* lysate (0.5 h/2 h, light/dark blue). (b−g) Averaged SERS spectra from each treatment class (lower, blue) and VAE-generated spectra from the center of the class centroid (upper, orange): (b) [−] 0.5 h, (c) [+C] 0.5 h, (d) [+R] 0.5 h, (e) [−] 2 h, (F) [+C] 2 h, and (g) [+R] 2 h.

below the MIC_{50} determined from growth assays. These assays are shown in Figure S1. Lysate from *P. aeruginosa* and *E. coli* exposed to 10 μg/mL gentamicin, approximately 10 × MIC_{50}, is analyzed with SERS + deep learning and can begin to be differentiated from control data in the VAE space as early as 10 min after initial exposure (Figure 2b,d). This is much earlier than previously reported for SERS AST, where differentiation begins as early as 1 h.[36] Note that while data differentiation is observed between short time intervals after antibiotic treatment, sample preparation is required to obtain the SERS spectra, and approximately 1 h elapses between treatment and measurement.

A support vector machine (SVM), a discriminative model, was trained on both pre-processed spectra and VAE-encoded spectra. Figure S5 shows the classification accuracy of the SVM model of pre-processed and VAE-encoded spectra for the dose and temporal datasets as a function of training examples where an example is composed of one spectrum per class. We find that SVM analysis of VAE-encoded spectra performs much better than analysis of pre-processed spectra demonstrating the performance of the VAE for unsupervised data encoding and visualization. A classification accuracy in discriminating between the different dose and temporal conditions approaches 85% with 10 labeled samples, as shown in Figure S5b−e. It has previously been reported that SVM analysis of SERS spectra processed with principal component analysis was not adequate to differentiate variations in different classes from variations in similar classes in the complex spectral data.[66] While the VAE encoding improves SVM classification performance, the VAE parameters are fit to improve the reconstruction of input data, and not to reduce misclassification. Rapid AST would benefit from higher accuracy.

In order to more accurately determine the dosage and time point at which differentiating the SERS spectra becomes possible, we use a deep neural network (DNN) model, a supervised learning approach, to classify the spectra from *E. coli* and *P. aeruginosa* lysate with respect to their temporal and gentamicin dosage treatment conditions. In order to avoid overfitting, the dataset was doubled in size, which increased data collection time by less than 4 min. The DNN is trained directly on the raw spectral data and we develop multiple two-class DNN models with groupings of consecutive treatment conditions. For example, one experiment for the temporal datasets would classify the 0 and 5 min treatment conditions

(first class) against the 10, 20, and 40 min treatment conditions (second class). The resultant classification accuracy of these experiments are 99% ± 0.1% for both *E. coli* and *P. aeruginosa*. Thus, we are able to detect bacterial response to antibiotics after 10 min with greater than 99% accuracy. Examining all two-class model results, Table S1 in Supporting Information, we can see that the two-class feed-forward DNN models are able to distinguish between all possible groupings of temporal conditions with near-perfect mean 10-fold cross validation accuracy greater than 99% even when grouping the 0 min temporal response alone in a class. Thus, after only 5 min, bacterial response to antibiotics is clearly evident in the SERS spectra. The DNN performed equally well on all possible groupings in the two class analysis of dosage-variant datasets, also shown in Table S1. Because the two-class models performed so well, we explored five-class models in order to analyze the performance of the DNN model for differentiating each individual condition.

The five-class models achieved comparable accuracy as can be seen from the confusion matrices for each of the models (Figure 3). For the *P. aeruginosa* time variant dataset, we were able to achieve a mean 10-fold cross validation classification accuracy of 99 ± 0.2%. For the dosage variant dataset, the model had a mean 10-fold cross validation classification accuracy of 98 ± 1.0%. The *E. coli* temporal and dosage datasets performed similarly well, with mean 10-fold cross validation classification accuracies of 99 ± 0.3% and 95 ± 1% respectively. Looking at the confusion matrices in Figure 3b,d for both temporal datasets, we can clearly see early differentiation with the model showing a strong ability to differentiate classes as early as 5 min. For both models trained on the dosage datasets, we see clear differentiation with dosages as low as 0.1 μg/mL. It is important to note that the majority of misclassification results are for similar dosages or time points and thus SERS data is able to measure bacterial response below the MIC and track the temporal evolution of the bacterial response on a time scale of 5 min with high accuracy. Classification accuracy, equal to sensitivity, is considered the primary metric in this work since the goal of rapid AST is accurate antibiotic treatment. The relationships between the accuracy values listed in Figure 3 with specificity as well as sensitivity are provided in Tables S1 and S2.

While Figure 3 demonstrates high predictive accuracy with DNN discriminative models when analyzing SERS data as a

function of antibiotic dosage and exposure time of susceptible *P. aeruginosa* and *E. coli*, it is important to demonstrate that the SERS + deep learning methods are sufficiently robust to differentiate between resistant and susceptible antibiotic responses. SERS spectra of cell lysate from *P. aeruginosa* cultures were collected as a function of exposure time and type of antibiotic. The *P. aeruginosa* strain, PA14, used here, has differing susceptibility to carbenicillin [+C] and rifampicin [+R]. We refer to this data as the AST dataset, where the antibiotic treatments are performed with 50 and 400 μg/mL of carbenicillin and rifampicin, respectively. These concentrations are just below the respective measured MIC_{50} for these antibiotics in *P. aeruginosa* (see Figures S1 and S2).

At these concentrations, *P. aeruginosa* does not exhibit any significant growth inhibition over the maximum time of exposure, 2 h, used for lysate preparations (Figure S2). The VAE is trained on the AST dataset and shows clear clustering of the different treatment classes (Figure 4a), albeit with some variances within sample classes and anisotropy of clusters. Comparison of VAE generated (*i.e.*, decoded) spectra (blue curves) to averaged SERS spectra (orange curves) are shown in Figure 4b−g. The striking similarity between generated and experimental spectra confirms that the clustering behavior reflects trends in the experimental data. Additionally, while the SERS spectra is pre-processed, the VAE de-noises the spectra even further. This is evident as the VAE generated spectra are nearly indistinguishable from the averages of experimental spectra. In agreement with previous work, many of the spectral features in Figure 4b−g overlap with features associated with nucleotide degradation metabolites.[35,37,67] This has been attributed to an increase in nucleotide turn over which could be indicative of higher level of DNA damage.[20] Recently, nucleotide pool disruption has been correlated with antibiotic lethality network models and biochemical screening.[68]

When examining the observed clustering in VAE space, there is a clear observable trend of cell viability across VAE 2, with small VAE 2 values corresponding to untreated bacteria [−], intermediate VAE 2 values corresponding to treatment with rifampicin [+R], and large VAE 2 values corresponding to treatment with carbenicillin [+C]. The control data time evolution, shown as light and dark green squares in Figure 4, provides a reference for how the SERS spectra from lysate evolve over time for untreated bacteria. This trend tracks with the expected efficacy of each treatment, with rifampicin being intermediate between the control and carbenicillin treatment due to the evident resistance of *P. aeruginosa* to rifampicin (Figure S1). The appearance of this trend in the VAE space is notable, highlighting the ability of the SERS sensors to successfully differentiate these samples, particularly since all antibiotic treatments are below their respective MIC and hence do not inhibit growth over the time scale of exposure investigated here (Figure S2). It is interesting that larger relative VAE 1 values are observed for 30 min treatment times for both treatment classes as compared to 2 h exposure. This is consistent with OD_{600} measurements indicating cell recovery after 2 h in Figure S2. The reason for this trend requires further investigation, but may be a result of a relative recovery of normal metabolic activity at these sub-inhibitory concentrations after dysregulation of cellular metabolism on short time scales following initial exposure.[20,21,23] Figure S3 depicts a t-stochastic neighbor embedding (t-SNE) visualization of the spectra used to build the VAE latent spaces depicted in Figure 4. t-SNE is an unsupervised model that prioritizes preserving

the neighboring distances of spectral data points when reducing the dimensionality for visualization. The clear clustering illustrated by t-SNE affirms the conclusion of the VAE, that there are differences in the SERS spectra of *P. aeruginosa* exhibiting a resistant or susceptible response to antibiotic treatments that are identifiable using unsupervised algorithms.

The classification accuracy of the pre-processed and VAE-encoded spectra for the AST dataset as a function of training examples was also analyzed using a SVM and is shown in Figure S5a. We find again that SVM analysis of VAE-encoded spectra performs much better than analysis of pre-processed spectra. A classification accuracy in discriminating between the six antibiotic treatment conditions of the AST dataset of 83.7 ± 2.6% is achieved for the former case with approximately 10 labeled samples generated from growth assays, as shown in Figure S3a. This is compared to a performance of 72.9 ± 5.2% with a SVM trained on spectra that have not been encoded. While the improvement in accuracy with the VAE encoding is notable, below we examine methods to increase accuracy without requiring increased amounts of labeled data.

Data-Informed Transfer Learning for SERS AST. From a machine learning perspective one can consider conventional growth assays as a means of generating labels for response of bacteria to different antibiotic exposure conditions, and the SERS spectra as the resultant labeled data. The huge mismatch between the time for label generation and data generation, however, provide strong motivation for investigating semi-supervised and transfer learning approaches for classification. The correspondence between the VAE-encoded SERS spectra and the antibiotic treatment classes (Figure 4) indicates that a semi-supervised approach of the VAE latent space is a promising solution. The SVM analyses of VAE generated spectra indeed produce higher accuracy than analyses on uncoded spectra. Yet the desire for higher accuracy for clinical applications without increasing the demand for more training data motivates the investigation of training models from easily acquired unlabeled data to reduce the time for creating labels. Traditional transfer learning with deep neural networks is done by training a model, such as a convolutional neural network (CNN) with a large dataset, and then fine-tuning the model's parameters with a smaller dataset and has been shown to improve model predictions such as classification accuracy.[49,66] The use of a generative machine learning method enables us to take an informed approach to transfer learning. For example, the high interpretability of the VAE generated SERS spectra allows us to identify useful vibrational information which guides additional targeted data collection to improve classification accuracy. We refer to this approach as *data-informed transfer learning* to differentiate from traditional transfer learning. By sampling 100 VAE generated spectra between the average response of the untreated 2 h lysate data and that of the 0.5 h carbenicillin-treated lysate data plotted in Figure 4a, it is possible to visualize how spectral features shift as a result of antibiotic exposure (Supporting Video 1). This progression shows that the bacterial lysate response to antibiotics exhibits changes in the 1100−1200 cm^{-1} bands. Aromatic functional groups have vibrational features in this frequency range and provide an easy to acquire unlabeled dataset for algorithm training. It is important to mention that our method does not seek to identify or quantify specific metabolites produced by the bacteria in response to antibiotic treatment conditions. It is designed to use the overall

differences in metabolic profile as an assessment of antibiotic susceptibility observed in other fingerprinting technology[69,70] and thus making it generalizable to variations in bacterial strain response. Based on these observations, six generic, volatile aromatic bacterial metabolites—2-methylnaphthalene, o-cresol, 2-aminoacetophenone, pyrrole, 2-pentylfuran, and indole[71]— were selected to construct a "metabolite mixture" dataset to use for data-informed transfer learning. This dataset was generated by collecting SERS spectra from all 63 aqueous solution combinations of between 1 to all 6 of these metabolites at a total concentration of 1 ppm. This approach of producing easy-to-collect spectra (large, metabolite mixture dataset) based on observations of difficult-to-collect spectra (cell culture AST dataset) is an extremely beneficial aspect of data-informed transfer learning for SERS analysis, and we depict the virtuous cycle that results in Scheme 1. The

Scheme 1. Cycle of Data-Informed Transfer Learning[a]
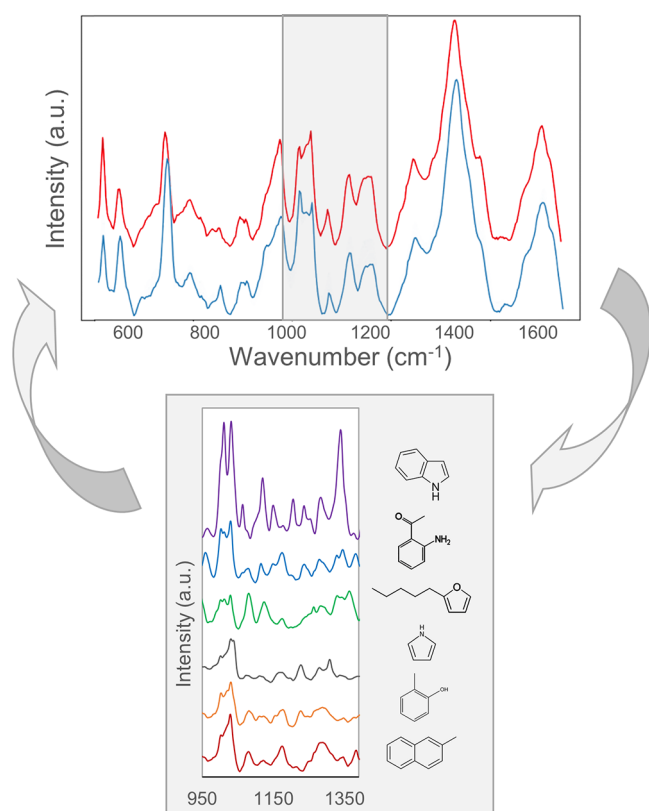
[a]Top: VAE-encoded spectra of *P. aeruginosa* lysate 0.5 h after being treated with carbenicillin (blue curve) and 2 h untreated (red curve). In order to dramatically improve the classification performance of the AST dataset, we take advantage of this information provided by VAE encoding to select a metabolite mixture dataset to further expand the training of the VAE latent space. Bottom: SERS spectra of (from bottom to top) 2-methylnaphthalene, o-cresol, pyrrole, 2-pentylfuran, 2-aminoacetophenone, and indole at concentrations of 1 ppm.

metabolite data, which has vibrational modes producing spectral features in the frequency range of interest, expands the VAE space and produces bigger differences between the encodings of the AST dataset, resulting in improved classification accuracy as we discuss below. This approach is motivated by works in natural language processing, where training on large unsupervised datasets has led to improved encodings and downstream model performance.[72]

This combined VAE latent space of metabolite mixtures and AST dataset is also depicted in Figure S6a; it is constrained to two dimensions so that it can be easily examined. The improved clustering, even in two dimensions, of the AST dataset with respect to Figure 4a is observed in the center right side of Figure S6a (highlighted with an arrow). Overall these results demonstrate that culture-free and easily acquired datasets of bacterial metabolites in aqueous solution can be leveraged to improve predictive models of complex metabolite response of bacterial communities and is one of the most significant advantages of using a generative model.

From here, it is straightforward to build a predictive model. First, the VAE encoding makes it obvious that some of the spectra are outliers. These spectra are easily removed with an isolation forest set to remove 5% of spectra, detailed in the Supporting Information and shown in Figure S7. An unsupervised Bayesian Gaussian mixture model of the outlier removed AST dataset encoded with the combined VAE visualizes the classification accuracy in Figure 5a. Highly accurate identification of the different classes, 99.3%, is achieved for only one training example; the only information given to the model is that the number of classes to expect is six. Figure 5a shows that the combined VAE encoding nicely groups the different antibiotic conditions together with only one cycle. This clear clustering with a pre-trained model and only one labeled training example will benefit applications for AST analysis of clinical datasets. Finally, we further motivate the significance of the presented data-informed transfer learning approach by comparing the number of labeled examples needed with traditional transfer learning to achieve similar accuracy. Traditional transfer learning is performed here by taking the six unmixed metabolite datasets (*i.e.*, 2-methylnaphthalene, o-cresol, 2-aminoacetophenone, pyrrole, 2-pentylfuran, and indole dissolved in water by themselves) and training a model with those spectra. The weights of these trained networks are then fine-tuned with the AST dataset.

Two models are compared, a multilayer perceptron (MLP, orange triangles), which is a fully connected artificial neural network with one hidden layer and a CNN (blue circles), which is composed of four 1D CNN layers. The MLP is trained with VAE-encoded data and the CNN is trained with pre-processed SERS spectra without VAE encoding. The architecture and training details are described in the Methods. This procedure is performed 10 times for each example number. The resultant mean and standard deviation of the model accuracy are plotted in Figure 5b as a function of the number of training examples. In addition to comparing these CNN and MLP models with random parameter initialization, we also use traditional transfer learning for both models, where the six unmixed metabolite datasets are used to train a predictive model and then fine-tuned with examples from the AST datasets as performed with the non-transfer-learned models, yielding the transfer-learned CNN (green squares) and transfer-learned MLP (red diamonds). Interestingly, the transfer-learned MLP (red diamonds) is determined to produce the best predictions for one-shot learning, with transfer-learned CNN (green squares) approaching similar performance as this MLP model for three examples. The mean accuracy and standard deviation approach 98.5% and 1.1%, respectively, for 10 examples for the transfer-learned MLP model. From Figure 5b it is obvious that CNNs are an incredibly powerful tool for classifying SERS spectra. For reference, even without transfer learning, a CNN achieves
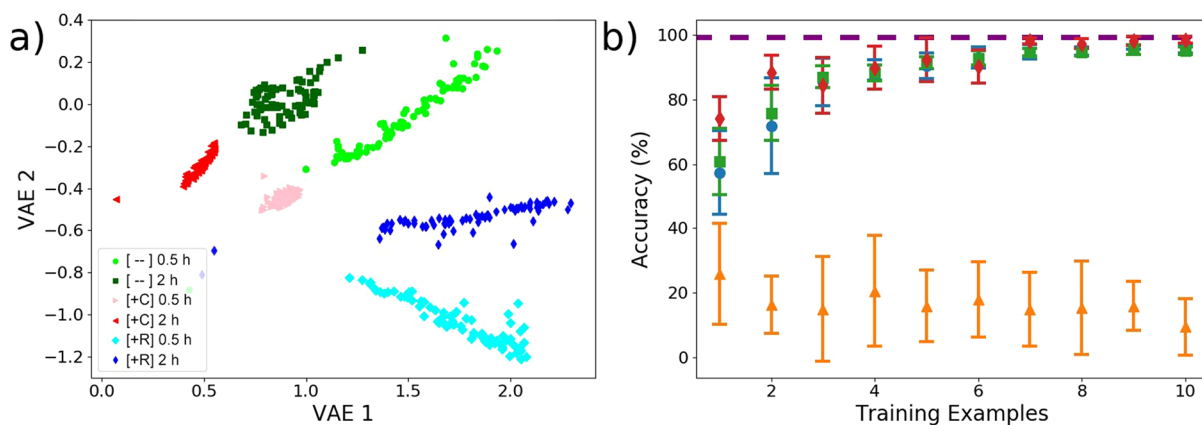
Figure 5. (a) Bayesian Gaussian mixture analysis of data-informed VAE-encoded *P. aeruginosa* AST test spectra. (b) Comparison of different models' performance as a function of number of training examples. Each model is evaluated 10 times, and the standard deviation is plotted along with the mean prediction accuracy. Transferred model CNN (green squares) and MLP (red diamonds) weights are trained using the unmixed metabolite dataset and fine-tuned with examples from the AST dataset, and then model classification accuracy is evaluated on test spectra. The same architectures, CNN (blue circles) and MLP (orange triangles), are evaluated without transfer learning using standard Xavier weight initialization for comparison. The inputs for CNN models are pre-processed SERS spectra, and the inputs for MLP models are spectra encoded using the combination VAE. The unsupervised Bayesian Gaussian mixture method (depicted as purple dashed line) achieves the highest accuracy at 99.3% with only one training example.

good results with just four examples (blue circle) far better than MLP (orange triangle) without transfer learning. Transfer learning with the CNN improves classification accuracy regardless of the number of examples but the difference is most pronounced with few examples. Importantly, none of these models outperforms our data-informed transfer learning approach using the simple Bayesian Gaussian mixture model discussed above.

CONCLUSION

We have demonstrated that the response of *P. aeruginosa* and *E. coli* bacterial communities to antibiotics is rapidly detected in SERS spectral data when using sensor surfaces with controlled nanogap spacing and chemistry. A VAE—a self-supervised deep generative machine learning model—has well-behaved latent space and produces clusters of SERS spectra that differentiate untreated cells from antibiotic-stressed cells. Deep learning analysis of SERS data is able to differentiate the response of untreated cells from those exposed to antibiotics in 10 min post exposure with greater than 99% accuracy and temporally follow the evolution with 5 min resolution with greater than 99% accuracy, significantly faster and more accurate than current SERS AST methods.[38,73,74] The bacterial response to varying antibiotic doses is differentiated with greater than 96% accuracy from untreated bacteria, even when treated with antibiotic dosages up to 10-fold lower than the minimum inhibitory concentration observed in conventional growth assays. Furthermore, the generative nature of the VAE enables facile visualization of the important vibrational features differentiating resistance *versus* susceptibility to antibiotics within the SERS spectra in the frequency range associated with vibrational modes of aromatic rings. A dataset of mixtures of metabolites in aqueous solution with similar vibrational features is chosen for *data-informed transfer learning*. This additional unlabeled training data greatly improves the classification accuracy of the SERS AST spectra. Unsupervised Bayesian Gaussian mixture analysis achieves 99.3% classification accuracy differentiating susceptibility *versus* resistance to antibiotics when a single spectrum from each category is used

as an input. These results show that the need for time-consuming 24+ hour cell culture, which is necessary to generate labels for training SERS AST, can be minimized, along with sample volume, when using 2PAC SERS sensors + deep learning based AST. One can foresee that analysis when conducted with data-informed transfer learning can look at a small number of labeled samples from individual patients, and that the response of susceptible bacteria to antibiotics can be detected before observable changes in cell growth assays, in under 90 min. The high classification accuracy/sensitivity and specificity in following temporal response of monocultures and differentiating susceptibility and resistance demonstrates the SERS + deep learning approach described here makes this method a promising candidate for use in clinical samples for rapid AST. In future works, we seek to use these methods to analyze bacterial heteroresistance in polymicrobial samples, which we view as one of the key challenges for SERS AST to overcome in order to be used in a clinical setting.

METHODS

Materials. Random copolymer poly(styrene-*co*-methyl methacrylate)-*α*-hydroxyl-*ω*-tempo moiety (PS-r-PMMA) (M_n = 7400, 59.6% PS) and diblock copolymer poly(styrene-*block*-methyl methacrylate) (PS-*b*-PMMA) (M_n = 170-*b*-144 kg mol^{-1}) were purchased from Polymer Source, Inc. (Dorval, Canada). 40 nm diameter lipoic acid functionalized gold nanospheres were purchased from Nanocomposix (San Diego, CA). Si(001) wafers with a resistivity of 0.004 Ω·cm were purchased from Virginia Semiconductor (Frederickburg, VA). Hydrofluoric acid (HF) was purchased from Fisher Scientific (Pittsburgh, PA). 2-(*N*-Morpholino)ethanesulfonic acid (MES) 0.1 M buffer, 1-ethyl-3-[3-(dimethylamino)propyl]carbodiimide hydrochloride (EDC), *N*-hydroxysulfosuccinimide (s-NHS), dimethyl sulfoxide (DMSO), ethylenediamine, benzenethiol, toluene, ethanol, isopropyl alcohol (IPA), potassium carbonate, and 52-mesh Pt gauze foil were purchased from Sigma-Aldrich (St. Louis, MO). Nanopure deionized (DI) water (18.2 MΩ cm^{-1}) was obtained from a Milli-Q Millipore System. LB Lennox and bacteriological agar were purchased from IBI Scientific (Dubuque, IA). Carbenicillin disodium salt was purchased from Sigma-Aldrich (St. Louis, MO). Gentamycin sulfate was purchased from VWR Life Science (Radnor, PA). Rifampicin was purchased from Frontier Scientific (Logan, UT). Dimethyl sulfoxide was also purchased from Alfa Aesar (Haverhill, MA). Phosphate

buffer solution (pH = 7.4) was purchased from Fisher Scientific (Waltham, MA).

Surface-Enhanced Raman Scattering (SERS) Sensor Fabrication. Sensor fabrication has been described in depth in previous work.[29] First, we prepare block copolymer templates for Au nanosphere assembly attachment. Random PS-*b*-PMMA block copolymer is spin-coated onto a HF-cleaned Si wafer and annealed for 72 h. [*Caution: HF has serious potential to cause severe injury which mandates extreme care during treatment.*] The wafer is rinsed with toluene, and lamella-forming PS-*b*-PMMA block copolymer is spin-coated onto the wafer, which is annealed for another 72 h. This process is described elsewhere.[75] Next, PMMA regions within the block copolymer are selectively functionalized with amine terminated end groups by immersing a 1 cm × 1 cm piece of the wafer in DMSO. This substrate is then transferred into an ethylenediamine/DMSO solution (5% v/v). Both immersions are performed for 5 min without rinsing between steps. The functionalized template is then rinsed with IPA for 1 min and dried under nitrogen for immediate use.

An electrohydrodynamic flow-driven assembly of Au nanospheres is used to generate assemblies with the following method: Au nanosphere solution (0.1 mg/mL, 3 mL) is added to a clean 10 mL glass beaker. s-NHS (20 mM) in MES (0.1 M) buffer (35 μL) is added to the nanosphere solution and swirled. Next, EDC (8 mM) in MES (0.1 M) buffer (35 μL) is added to this solution and swirled. The solution is brought to and maintained at 60 °C with a hot plate. The functionalized block copolymer-coated Si substrate is placed vertically into the solution and held in place with alligator clips, taking care to avoid any contact of the alligator clips with the solution. A 1 cm × 1 cm Pt mesh is placed in parallel 1 mm away from the substrate. 1.2 V is applied across the mesh and substrate using a DC power supply for 10 min. Everything is then rinsed with IPA for 1 min and dried under nitrogen. The process is repeated with the same substrate and a fresh nanosphere solution, but with 25 μL of s-NHS and EDC solution.

Bacterial Culture Preparation. *Pseudomonas aeruginosa* (strain PA14 wild type) and *Escherichia coli* (strain MC4100, K-12, F−araD139Δ(*argF-lac*)U169 *rspL150 relA1 flbB5301 fruA25 deoC1 ptsF25*)[76] cultures were revived by streaking from a frozen culture stock onto LB Lennox agar (IBI Scientific) plates and incubated at 37 °C for 24 h. Individual colonies from these plates were used to inoculate solutions of 100 mL of LB in triplicate, which were subsequently grown for 18 h at 37 °C and shaking at 230 rpm. The 18 h cultures were centrifuged at 5000 rpm for 5 min, then re-suspended in fresh LB at an optical density at 600 nm (OD_{600}) of 0.50 as measured by a BioChrom Colourwave CO7500 colorimeter.

Antibiotic Dose−Response Curves. Carbenicillin disodium salt (Sigma-Aldrich), gentamicin sulfate (VWR Life Science), and rifampicin (Frontier Scientific) stock solutions were prepared to a final concentration of 10 mg/mL in water for the former two and 20% (v/v) DMSO (Alfa Aesar)/ H_2O for the latter. These stock solutions were diluted and 20 μL each added into 180 μL of *E. coli* or *P. aeruginosa* re-suspension in a 96-well plate such that nine separate 10-fold dilutions of each antibiotic starting at 1000 μg/mL final concentration in the culture were achieved. Vehicle controls using pure water for carbenicillin and gentamicin and 20% (v/v) DMSO/ H_2O for rifampicin were also created in the same 96-well plate. These plates were then incubated at 37 °C for 24 h with 230 rpm shaking, after which OD_{600} measurements were taken with a SpectraMax M2 Plate Reader (Nova Biotech).

Antibiotic Exposure. Cell re-suspensions of 40 mL in 50 mL conical tubes were treated with specified concentration of antibiotics for the indicated time in a shaking incubator at 37 °C and 230 rpm.

Lysate Extraction. After the specified time of growth, cell cultures were washed twice with phosphate buffer solution (PBS, Fisher Scientific, pH = 7.4) by centrifugation at 5000 rpm for 5 min and re-suspension in 40 mL of PBS. After the second wash, the cells were pelleted a third time and then re-suspended in 100 μL of sterile ultrapure water and heated at 100 °C for 30 min. The resulting suspension was centrifuged at 12 000 rpm for 10 min, and the

supernatant was collected and stored at −20 °C for subsequent SERS analysis.

Metabolite Mixture Preparation. Metabolite mixtures are prepared as follows: 2-methylnapthalene, *o*-cresol, 2-amino-acetophenone, pyrrole, 2-pentylfuran, and indole are dissolved in ethanol at a concentration of 100 ppm. Then 1 ppm solutions are prepared in water from these ethanol stock solutions. The 63 combinations of metabolites are prepared by mixing the water stock solutions to maintain a total metabolite concentration of 1 ppm.

SERS Spectroscopy. All SERS spectroscopy measurements are conducted using a confocal Renishaw InVia micro Raman system with a 785 nm diode laser, a laser power of 14 μW, an exposure time of 0.5 s, and a 60× water immersion objective with a 1.2 numerical aperture. Bacteria cell lysate or metabolite mixture solutions are used as the immersion media. After soaking the SERS substrate in the sample for 15 min, Raman maps are collected with a spacing of 4 μm spacing between points. For each sample one 20 × 20 pixel Raman map is acquired.

Spectra Pre-processing. Spectra are pre-processed in three steps: (1) smoothing, (2) background subtraction, and (3) scaling, all done using the Python 3.3 programming language. Smoothing was done with the Savitzky−Golay method[77] as implemented in Scikit-Learn using an 11 pixel window and polynomial order 3. Background subtraction was done with the asymmetric least-squares method[78] and was implemented in NumPy with λ = 10000, *p* = 0.001. Spectra were scaled to have a minimum value of 0 and maximum value of 1 with Scikit-learn's MinMaxsScaler.

Feed-forward Deep Neural Network. The four datasets used in these experiments (*E. coli* temporal, *E. coli* dose, *P. aeruginosa* temporal, and *P. aeruginosa* dose) were all pre-processed using the spectra pre-processing method outlined above. 800 spectra from each condition are used to train the model. The DNNs were trained using 10-fold cross validation. For each cross fold the data was divided into a training, validation, and test set. As a supervised machine learning method, training data is used to fit the parameters of the DNN; knowledge of the class that each point of training data belongs to is necessary. The validation set for each cross fold is unique and is a random 20% subset of the training set of that cross fold. The DNNs used in this study are feed-forward layered networks with fully connected layers and a logistic output for the two-class models or a softmax output for the five-class models. We used the python hyperparameter optimization library SHERPA in combination with 10-fold cross validation to select the best hyperparameters and architecture based on mean cross validation accuracy.[79] All of the models utilize the Adam optimizer with a learning rate of 0.001 and a batch size of 20. The DNN architectures used have 1−3 hidden layers with 10−500 neurons per layer, and rectified linear unit (ReLU) activation functions. The loss function used for the two-class models was binary cross entropy and the loss function used for the five-class models was categorical cross entropy. Due to the relatively small number of samples compared to the very large number of features, we use Scikit-learn to perform principal component analysis (PCA) with an explained variance of 99% for dimensionality reduction.

In order to avoid overfitting, we used early stopping in combination with data augmentation. Early stopping is a technique used to halt model training when the loss of the validation set starts to increase compared to the training loss, indicating overfitting. For our experiments, we used a patience of 10. Additionally, in some of the networks we utilized dropout and L2 regularization to combat overfitting. For data augmentation we used the Synthetic Minority Oversampling Technique (SMOTE) to combat the problem of class imbalance.[80] Although the original dataset does not have significant class imbalance between the five classes, when we split the data into two groups for our two-class models we introduced class imbalance. For example, one of the two-class models is 0 min, 5 min, 10 min, 20 min as one class (3200 data points) and 40 min as one class (800 data points). SMOTE augments the data by synthesizing training examples in the minority class. Specifically, SMOTE chooses a random data point from the minority class and a random neighbor from its five nearest neighbors, and then a synthetic example is created at a

randomly selected point between the two examples in feature space. Data augmentation was only performed on the training set; the test set was not augmented.

To measure the performance of each of the models, we used 10-fold mean cross validation accuracy.

Variational Autoencoder Implementation. All artificial neural network models are implemented in keras and use the adam optimizer.[66]

Prior to use in the variational autoencoder[81] (VAE), spectra are pre-processed as described above. These 1011 dimensional spectra are padded with zeros to 1024 dimensions and reshaped to a dimension of examples (1024, one for use in one-dimensional convolutional neural network (1D CNN) layers). All 1D CNN layers have a kernel window of 8 pixels, a stride of 2, are regularized with a maximum kernel norm of 3, have parametric ReLU activations, are batch normalized, and followed with a 30% dropout layer. Early stopping is implemented with test loss, and the batch size used is 32. VAE models use a loss function defined as KL divergence + mean absolute error * 80. A total of 400 spectra from each condition are used to train the VAE, with 20% of the spectra randomly removed from the training dataset and used as the test dataset. We do not condition the VAE space on condition labels (*e.g.*, 0.5 h control, 2 h rifampicin, *etc.*), so we implement the VAE here as a fully self-supervised method.

The VAE is implemented differently for the antimicrobial susceptibility testing (AST) dataset and the AST and metabolite mixture combined dataset. For the smaller AST dataset, the encoder network is composed of 4 1D CNN layers with 32, 32, 64, and 64 filters. This output is flattened and sent to a 128-node fully connected layer with parametric ReLU activation, batch normalization, and 30% dropout and sent to a 32-node fully connected layer with parametric ReLU activation, and finally to fully connected layers with two nodes that represent the mean and standard deviation of the encoded input. The decoder is similar, with a 1344-node fully connected layer, reshaped and sent to four 1D transposed CNN layers with 64, 64, 32, and 32 filters. This is output to a 1D transposed CNN with stride 1, sigmoid activation, and a stride of 1.

For the larger combined dataset, the encoder network is composed of six 1D CNN layers with 32, 32, 64, 64, 128, and 128 filters, with 40% dropout. This output is flattened and sent to a 256 node fully connected layer with parametric ReLU activation, batch normalization, and 50% dropout and sent to a 64 node fully connected layer with parametric ReLU activation, and finally to fully connected layers with two nodes that represent the mean and standard deviation of the encoded input. The decoder is similar to a 2048 node fully connected layer, reshaped and sent to eight 1D transposed CNN layers with 256, 256 (stride 1), 256, 256 (stride 1), 128, 128, 64, and 64 filters. This is output to a 1D CNN with one filter, sigmoid activation, and a stride of 1.

Semi-supervised Learning Using Support Vector Machines. The models in Figure S3 are evaluated as follows. Examples (one pre-processed SERS spectrum per class) are pulled from the test dataset used in training the VAE described above. These are used to train support vector machine (SVM) models with Scikit-learn using default settings. The SVM models are trained using pre-processed spectra with dimension 1011 and the accuracy is evaluated using the rest of the test dataset. The VAE SVM models were evaluated with the same examples projected into the latent space of the trained AST VAE and evaluated with the same dataset. This process is done 50 times and the mean and standard deviation of the model accuracy on the remaining spectra are depicted.

Transfer Learning. This section describes the methods used to produce Figure 5. First for data-informed transfer learning, after analyzing the AST dataset and highlighting features with large variations between categories, the AST and metabolite dataset are encoded into a two-dimensional latent space producing a combined VAE. Outliers are removed by training an isolation forest[82] on the training dataset. Isolation forest is implemented in Scikit-learn with the default settings and an outlier fraction of 5%. The outlier removed training dataset is then used to train a Bayesian Gaussian mixture model, which is implemented in Scikit-learn with the default settings

and six components,[83] and evaluated on the test dataset, where on training example is a single processed SERS spectra per category. The results of Bayesian mixture analysis is plotted in Figure 5a.

Traditional transfer learning is performed by taking the six unmixed metabolite datasets (*i.e.*, 2-methylnaphthalene, *o*-cresol, 2-amino-acetophenone, pyrrole, 2-pentylfuran, and indole dissolved in water by themselves) and training a model with those spectra. The weights of these trained networks are then fine-tuned for various numbers of examples from the AST dataset, where each example is composed of SERS spectra, one from each category. The neural network models evaluated in Figure 5b are evaluated with categorical cross entropy loss and have the following architectures. (1) The first network model is a deep CNN trained on the full dimensional pre-processed data and is composed of four 1D CNN layers with filters of 16, 16, 32, and 32 that are followed by 50% dropout layers and batch normalized. This output is flattened and set to a six-node fully connected layer with softmax activation. (2) The second network model is a multilayer perceptron, which is composed of two fully connected layers with 8 and 16 nodes with ReLU activation and batch normalization. This output is sent to a fully connected layer with six nodes and softmax activation. It is trained on the VAE-encoded unmixed metabolite dataset, and then the weights are fine-tuned with the AST dataset with outlier spectra removed.

Additionally, these CNN and MLP network models are evaluated without transfer learning for comparison using only the AST dataset with standard Xavier initialization of the weights. The accuracy of all the models are evaluated, as a function of the number of examples and repeated 10 times per example number to obtain a mean and standard deviation of the model accuracy and plotted in Figure 5b. MLP, without transfer learning, does not yield good predictions from the VAE space, likely due to underfitting as there are only two features.

ASSOCIATED CONTENT

Ⓢ Supporting Information

The Supporting Information is available free of charge at https://pubs.acs.org/doi/10.1021/acsnano.0c05693.

> Figures S1 and S2, OD$_{600}$ data to identify the minimum inhibitory concentration of various antibiotics for *P. aeruginosa* and *E. coli* and growth assays of *P. aeruginosa* cell culture after exposure to carbenicillin and rifampicin at concentrations below the minimum inhibitory concentration; Figures S3 and S4, t-SNE visualization of dose and temporal response of *P. aeruginosa* and *E. coli* exposed to the same antibiotic, and of *P. aeruginosa*, after exposure to different antibiotic treatments, and *E. coli*; Tables S1 and S2, two-class DNN model validation accuracies and the sensitivity and specificity of two-class and five-class DNN models; Figure S5, SVM model classification accuracy of dose and temporal response of *P. aeruginosa* and *E. coli* exposed to the same antibiotic, and SVM model classification accuracy of the AST dataset (*P. aeruginosa* untreated and treated with carbenicillin or rifampicin); Figure S6 and Table S3, visualization of the latent space of combined metabolite mixture and AST dataset; Figure S7, isolation forest predictions of outliers and inliers of SERS spectra in AST dataset (PDF)

> Supporting Video 1, showing generated spectra visualized in a trajectory across the latent space depicted in Figure 4 (MP4)

AUTHOR INFORMATION

Corresponding Author

Regina Ragan − *Department of Materials Science and Engineering and Department of Chemical and Biomolecular*

Engineering, University of California, Irvine, California 92697, United States; ● orcid.org/0000-0002-8694-5683; Email: rragan@uci.edu

Authors

William John Thrift − Department of Materials Science and Engineering, University of California, Irvine, California 92697, United States

Sasha Ronaghi − Sage Hill School, Newport Coast, California 92657, United States

Muntaha Samad − Department of Computer Science, University of California, Irvine, California 92697, United States

Hong Wei − Department of Materials Science and Engineering, University of California, Irvine, California 92697, United States

Dean Gia Nguyen − Department of Chemical and Biomolecular Engineering, University of California, Irvine, California 92697, United States

Antony Superio Cabuslay − Department of Chemistry, University of California, Irvine, California 92617, United States

Chloe E. Groome − Department of Materials Science and Engineering, University of California, Irvine, California 92697, United States

Peter Joseph Santiago − Department of Materials Science and Engineering, University of California, Irvine, California 92697, United States

Pierre Baldi − Department of Computer Science, University of California, Irvine, California 92697, United States; ● orcid.org/0000-0001-8752-4664

Allon I. Hochbaum − Department of Materials Science and Engineering, Department of Chemistry, Department of Chemical and Biomolecular Engineering, and Department of Molecular Biology and Biochemistry, University of California, Irvine, California 92697, United States; ● orcid.org/0000-0002-5377-8065

Complete contact information is available at:
https://pubs.acs.org/10.1021/acsnano.0c05693

Notes

The authors declare no competing financial interest.

REFERENCES

(1) Rochford, C.; Sridhar, D.; Woods, N.; Saleh, Z.; Hartenstein, L.; Ahlawat, H.; Whiting, E.; Dybul, M.; Cars, O.; Goosby, E.; Cassels, A.; Velasquez, G.; Hoffman, S.; Baris, E.; Wadsworth, J.; Gyansa-Lutterodt, M.; Davies, S. Global Governance of Antimicrobial Resistance. *Lancet* **2018**, *391* (10134), 1976−1978.

(2) Fleming-Dutra, K. E.; Hersh, A. L.; Shapiro, D. J.; Bartoces, M.; Enns, E. A.; File, T. M.; Finkelstein, J. A.; Gerber, J. S.; Hyun, D. Y.; Linder, J. A.; Lynfield, R.; Margolis, D. J.; May, L. S.; Merenstein, D.; Metlay, J. P.; Newland, J. G.; Piccirillo, J. F.; Roberts, R. M.; Sanchez, G. V.; Suda, K. J.; Thomas, A.; Woo, T. M.; Zetts, R. M.; Hicks, L. A. Prevalence of Inappropriate Antibiotic Prescriptions among US Ambulatory Care Visits, 2010−2011. *JAMA* **2016**, *315* (17), 1864−1873.

(3) Sugden, R.; Kelly, R.; Davies, S. Combatting Antimicrobial Resistance Globally. *Nat. Microbiol.* **2016**, *1* (10), 16187.

(4) O'Neill, J. *Tackling Drug-Resistant Infections Globally: Final Report and Recommendations*; Review on Antimicrobial Resistance, London, UK, May 2016.

(5) Pulido, M. R.; García-Quintanilla, M.; Martín-Peña, R.; Cisneros, J. M.; McConnell, M. J. Progress on the Development of Rapid Methods for Antimicrobial Susceptibility Testing. *J. Antimicrob. Chemother.* **2013**, *68* (12), 2710−2717.

(6) Reller, L. B.; Weinstein, M.; Jorgensen, J. H.; Ferraro, M. J. Antimicrobial Susceptibility Testing: A Review of General Principles and Contemporary Practices. *Clin. Infect. Dis.* **2009**, *49* (11), 1749−1755.

(7) Schoepp, N. G.; Schlappi, T. S.; Curtis, M. S.; Butkovich, S. S.; Miller, S.; Humphries, R. M.; Ismagilov, R. F. Rapid Pathogen-Specific Phenotypic Antibiotic Susceptibility Testing Using Digital LAMP Quantification in Clinical Samples. *Sci. Transl. Med.* **2017**, *9* (410), No. eaal3693.

(8) Holcomb, Z. E.; Tsalik, E. L.; Woods, C. W.; McClain, M. T. Host-Based Peripheral Blood Gene Expression Analysis for Diagnosis of Infectious Diseases. *J. Clin. Microbiol.* **2017**, *55* (2), 360−368.

(9) Marston, H. D.; Dixon, D. M.; Knisely, J. M.; Palmore, T. N.; Fauci, A. S. Antimicrobial Resistance. *JAMA* **2016**, *316* (11), 1193−1204.

(10) Baltekin, Ö.; Boucharin, A.; Tano, E.; Andersson, D. I.; Elf, J. Antibiotic Susceptibility Testing in Less than 30 min Using Direct Single-Cell Imaging. *Proc. Natl. Acad. Sci. U. S. A.* **2017**, *114* (34), 9170−9175.

(11) Figueiredo, S.; Bonnin, R. A.; Poirel, L.; Duranteau, J.; Nordmann, P. Identification of the Naturally Occurring Genes Encoding Carbapenem-Hydrolysing Oxacillinases from Acinetobacter Haemolyticus, Acinetobacter Johnsonii, and Acinetobacter Calcoaceticus. *Clin. Microbiol. Infect.* **2012**, *18* (9), 907−913.

(12) van Belkum, A.; Bachmann, T. T.; Ludke, G.; Lisby, J. G.; Kahlmeter, G.; Mohess, A.; Becker, K.; Hays, J. P.; Woodford, N.; Mitsakakis, K.; Moran-Gilad, J.; Vila, J.; Peter, H.; Rex, J. H.; Dunne, W. M. Developmental Roadmap for Antimicrobial Susceptibility Testing Systems. *Nat. Rev. Microbiol.* **2019**, *17* (1), 51−62.

(13) Nijhuis, R. H. T.; Guerendiain, D.; Claas, E. C. J.; Templeton, K. E. Comparison of EPlex Respiratory Pathogen Panel with Laboratory-Developed Real-Time PCR Assays for Detection of Respiratory Pathogens. *J. Clin. Microbiol.* **2017**, *55* (6), 1938−1945.

(14) Caliendo, A. M.; Hanson, K. E. Point-Counterpoint: The FDA Has a Role in Regulation of Laboratory-Developed Tests. *J. Clin. Microbiol.* **2016**, *54* (4), 829−833.

(15) Steingart, K. R.; Sohn, H.; Schiller, I.; Kloda, L. A.; Boehme, C. C.; Pai, M.; Dendukuri, N. Xpert MTB/RIF Assay for Pulmonary Tuberculosis and Rifampicin Resistance in Adults. *Cochrane Database Syst. Rev.* **2014**, *2014* (1), CD009593.

(16) Jung, J. S.; Hamacher, C.; Gross, B.; Sparbier, K.; Lange, C.; Kostrzewa, M.; Schubert, S. Evaluation of a Semiquantitative Matrix-Assisted Laser Desorption Ionization-Time of Flight Mass Spectrometry Method for Rapid Antimicrobial Susceptibility Testing of Positive Blood Cultures. *J. Clin. Microbiol.* **2016**, *54* (11), 2820−2824.

(17) Wimmer, J. L.; Long, S. W.; Cernoch, P.; Land, G. A.; Davis, J. R.; Musser, J. M.; Olsen, R. J. Strategy for Rapid Identification and Antibiotic Susceptibility Testing of Gram-Negative Bacteria Directly Recovered from Positive Blood Cultures Using the Bruker MALDI Biotyper and the BD Phoenix System. *J. Clin. Microbiol.* **2012**, *50* (7), 2452−2454.

(18) Burckhardt, I.; Zimmermann, S. Using Matrix-Assisted Laser Desorption Ionization-Time of Flight Mass Spectrometry to Detect Carbapenem Resistance within 1 to 2.5 h. *J. Clin. Microbiol.* **2011**, *49* (9), 3321−3324.

(19) Hrabák, J.; Walková, R.; Študentová, V.; Chudáčková, E.; Bergerová, T. Carbapenemase Activity Detection by Matrix-Assisted

Laser Desorption Ionization-Time of Flight Mass Spectrometry. *J. Clin. Microbiol.* **2011**, *49* (9), 3222−3227.

(20) Belenky, P.; Ye, J. D.; Porter, C. B. M.; Cohen, N. R.; Lobritz, M. A.; Ferrante, T.; Jain, S.; Korry, B. J.; Schwarz, E. G.; Walker, G. C.; Collins, J. J. Bactericidal Antibiotics Induce Toxic Metabolic Perturbations That Lead to Cellular Damage. *Cell Rep.* **2015**, *13* (5), 968−980.

(21) Dwyer, D. J.; Collins, J. J.; Walker, G. C. Unraveling the Physiological Complexities of Antibiotic Lethality. *Annu. Rev. Pharmacol. Toxicol.* **2015**, *55* (1), 313−332.

(22) Brynildsen, M. P.; Winkler, J. A.; Spina, C. S.; MacDonald, I. C.; Collins, J. J. Potentiating Antibacterial Activity by Predictably Enhancing Endogenous Microbial ROS Production. *Nat. Biotechnol.* **2013**, *31* (2), 160−165.

(23) Rowan, A. D.; Cabral, D. J.; Belenky, P. Bactericidal Antibiotics Induce Programmed Metabolic Toxicity. *Microb. Cell* **2016**, *3* (4), 178−180.

(24) Pozzi, F.; Zaleski, S.; Casadio, F.; Van Duyne, R. P. SERS Discrimination of Closely Related Molecules: A Systematic Study of Natural Red Dyes in Binary Mixtures. *J. Phys. Chem. C* **2016**, *120* (37), 21017−21026.

(25) Sun, D.; Cao, F.; Tian, Y.; Li, A.; Xu, W.; Chen, Q.; Shi, W.; Xu, S. Label-Free Detection of Multiplexed Metabolites at Single-Cell Level *via* a SERS-Microfluidic Droplet Platform. *Anal. Chem.* **2019**, *91* (24), 15484−15490.

(26) Lussier, F.; Missirlis, D.; Spatz, J. P.; Masson, J.-F. Machine-Learning-Driven Surface-Enhanced Raman Scattering Optophysiology Reveals Multiplexed Metabolite Gradients Near Cells. *ACS Nano* **2019**, *13* (2), 1403−1411.

(27) Plou, J.; García, I.; Charconnet, M.; Astobiza, I.; García-Astrain, C.; Matricardi, C.; Mihi, A.; Carracedo, A.; Liz-Marzán, L. M. Multiplex SERS Detection of Metabolic Alterations in Tumor Extracellular Media. *Adv. Funct. Mater.* **2020**, *30* (17), 1910335.

(28) Adams, S. M.; Campione, S.; Capolino, F.; Ragan, R. Directing Cluster Formation of Au Nanoparticles from Colloidal Solution. *Langmuir* **2013**, *29* (13), 4242−4251.

(29) Thrift, W. J.; Nguyen, C. Q.; Darvishzadeh-Varcheie, M.; Zare, S.; Sharac, N.; Sanderson, R. N.; Dupper, T. J.; Hochbaum, A. I.; Capolino, F.; Abdolhosseini Qomi, M. J.; Ragan, R. Driving Chemical Reactions in Plasmonic Nanogaps with Electrohydrodynamic Flow. *ACS Nano* **2017**, *11* (11), 11317−11329.

(30) Thrift, W. J.; Ragan, R. Quantification of Analyte Concentration in the Single Molecule Regime Using Convolutional Neural Networks. *Anal. Chem.* **2019**, *91* (21), 13337−13342.

(31) Thrift, W. J.; Cabuslay, A.; Laird, A. B.; Ranjbar, S.; Hochbaum, A. I.; Ragan, R. Surface-Enhanced Raman Scattering-Based Odor Compass: Locating Multiple Chemical Sources and Pathogens. *ACS Sens.* **2019**, *4* (9), 2311−2319.

(32) Bodelón, G.; Montes-García, V.; López-Puente, V.; Hill, E. H.; Hamon, C.; Sanz-Ortiz, M. N.; Rodal-Cedeira, S.; Costas, C.; Celiksoy, S.; Pérez-Juste, I.; Scarabelli, L.; La Porta, A.; Pérez-Juste, J.; Pastoriza-Santos, I.; Liz-Marzán, L. M. Detection and Imaging of Quorum Sensing in *Pseudomonas Aeruginosa* Biofilm Communities by Surface-Enhanced Resonance Raman Scattering. *Nat. Mater.* **2016**, *15* (11), 1203−1211.

(33) Galvan, D. D.; Yu, Q. Surface-Enhanced Raman Scattering for Rapid Detection and Characterization of Antibiotic-Resistant Bacteria. *Adv. Healthcare Mater.* **2018**, *7* (13), 1701335.

(34) Nguyen, C. Q.; Thrift, W. J.; Bhattacharjee, A.; Ranjbar, S.; Gallagher, T.; Darvishzadeh-Varcheie, M.; Sanderson, R. N.; Capolino, F.; Whiteson, K.; Baldi, P.; Hochbaum, A. I.; Ragan, R. Longitudinal Monitoring of Biofilm Formation *via* Robust Surface-Enhanced Raman Scattering Quantification of Pseudomonas Aeruginosa-Produced Metabolites. *ACS Appl. Mater. Interfaces* **2018**, *10* (15), 12364−12373.

(35) Premasiri, W. R.; Chen, Y.; Williamson, P. M.; Bandarage, D. C.; Pyles, C.; Ziegler, L. D. Rapid Urinary Tract Infection Diagnostics by Surface-Enhanced Raman Spectroscopy (SERS): Identification and

Antibiotic Susceptibilities. *Anal. Bioanal. Chem.* **2017**, *409* (11), 3043−3054.

(36) Chiu, S. W.-Y.; Cheng, H.-W.; Chen, Z.-X.; Wang, H.-H.; Lai, M.-Y.; Wang, J.-K.; Wang, Y.-L. Quantification of Biomolecules Responsible for Biomarkers in the Surface-Enhanced Raman Spectra of Bacteria Using Liquid Chromatography-Mass Spectrometry. *Phys. Chem. Chem. Phys.* **2018**, *20* (12), 8032−8041.

(37) Liu, C.-Y.; Han, Y.-Y.; Shih, P.-H.; Lian, W.-N.; Wang, H.-H.; Lin, C.-H.; Hsueh, P.-R.; Wang, J.-K.; Wang, Y.-L. Rapid Bacterial Antibiotic Susceptibility Test Based on Simple Surface-Enhanced Raman Spectroscopic Biomarkers. *Sci. Rep.* **2016**, *6*, 23375.

(38) Chang, K.-W.; Cheng, H.-W.; Shiue, J.; Wang, J.-K.; Wang, Y.-L.; Huang, N.-T. Antibiotic Susceptibility Test with Surface-Enhanced Raman Scattering in a Microfluidic System. *Anal. Chem.* **2019**, *91* (17), 10988−10995.

(39) Baldi, P. Deep Learning in Biomedical Data Science. *Annu. Rev. Biomed. Data Sci.* **2018**, *1* (1), 181−205.

(40) Hofer, I. S.; Lee, C.; Gabel, E.; Baldi, P.; Cannesson, M. Development and Validation of a Deep Neural Network Model to Predict Postoperative Mortality, Acute Kidney Injury, and Reintubation Using a Single Feature Set. *Npj Digit. Med.* **2020**, *3* (1), 58.

(41) Ershoff, B. D.; Lee, C. K.; Wray, C. L.; Agopian, V. G.; Urban, G.; Baldi, P.; Cannesson, M. Training and Validation of Deep Neural Networks for the Prediction of 90-Day Post-Liver Transplant Mortality Using UNOS Registry Data. *Transplant. Proc.* **2020**, *52* (1), 246−258.

(42) Baldi, P.; Chauvin, Y. Neural Networks for Fingerprint Recognition. *Neural Comput.* **1993**, *5* (3), 402−418.

(43) Esteva, A.; Kuprel, B.; Novoa, R. A.; Ko, J.; Swetter, S. M.; Blau, H. M.; Thrun, S. Dermatologist-Level Classification of Skin Cancer with Deep Neural Networks. *Nature* **2017**, *542* (7639), 115−118.

(44) Cheng, J.-Z.; Ni, D.; Chou, Y.-H.; Qin, J.; Tiu, C.-M.; Chang, Y.-C.; Huang, C.-S.; Shen, D.; Chen, C.-M. Computer-Aided Diagnosis with Deep Learning Architecture: Applications to Breast Lesions in US Images and Pulmonary Nodules in CT Scans. *Sci. Rep.* **2016**, *6*, 24454.

(45) Wang, J.; Ding, H.; Bidgoli, F. A.; Zhou, B.; Iribarren, C.; Molloi, S.; Baldi, P. Detecting Cardiovascular Disease from Mammograms With Deep Learning. *IEEE Trans. Med. Imaging* **2017**, *36* (5), 1172−1181.

(46) Urban, G.; Tripathi, P.; Alkayali, T.; Mittal, M.; Jalali, F.; Karnes, W.; Baldi, P. Deep Learning Localizes and Identifies Polyps in Real Time with 96% Accuracy in Screening Colonoscopy. *Gastroenterology* **2018**, *155* (4), 1069−1078.

(47) Urban, G.; Bache, K.; Phan, D. T. T.; Sobrino, A.; Shmakov, A. K.; Hachey, S. J.; Hughes, C. C. W.; Baldi, P. Deep Learning for Drug Discovery and Cancer Research: Automated Analysis of Vascularization Images. *IEEE/ACM Trans. Comput. Biol. Bioinf.* **2019**, *16* (3), 1029−1035.

(48) Chang, P.; Grinband, J.; Weinberg, B. D.; Bardis, M.; Khy, M.; Cadena, G.; Su, M.-Y.; Cha, S.; Filippi, C. G.; Bota, D.; Baldi, P.; Poisson, L. M.; Jain, R.; Chow, D. Deep-Learning Convolutional Neural Networks Accurately Classify Genetic Mutations in Gliomas. *Am. J. Neuroradiol.* **2018**, *39* (7), 1201−1207.

(49) Ho, C.-S.; Jean, N.; Hogan, C. A.; Blackmon, L.; Jeffrey, S. S.; Holodniy, M.; Banaei, N.; Saleh, A. A. E.; Ermon, S.; Dionne, J. Rapid Identification of Pathogenic Bacteria Using Raman Spectroscopy and Deep Learning. *Nat. Commun.* **2019**, *10* (1), 4927.

(50) Le Ru, E. C.; Meyer, M.; Etchegoin, P. G. Proof of Single-Molecule Sensitivity in Surface Enhanced Raman Scattering (SERS) by Means of a Two-Analyte Technique. *J. Phys. Chem. B* **2006**, *110* (4), 1944−1948.

(51) Alharbi, O.; Xu, Y.; Goodacre, R. Simultaneous Multiplexed Quantification of Nicotine and Its Metabolites Using Surface Enhanced Raman Scattering. *Analyst* **2014**, *139* (19), 4820−4827.

(52) Shi, H.; Wang, H.; Meng, X.; Chen, R.; Zhang, Y.; Su, Y.; He, Y. Setting Up a Surface-Enhanced Raman Scattering Database for Artificial-Intelligence-Based Label-Free Discrimination of Tumor Suppressor Genes. *Anal. Chem.* **2018**, *90* (24), 14216−14221.

(53) Li, J.; Skeete, Z.; Shan, S.; Yan, S.; Kurzatkowska, K.; Zhao, W.; Ngo, Q. M.; Holubovska, P.; Luo, J.; Hepel, M.; Zhong, C.-J. Surface Enhanced Raman Scattering Detection of Cancer Biomarkers with Bifunctional Nanocomposite Probes. *Anal. Chem.* **2015**, *87* (21), 10698−10702.

(54) Dong, R.; Weng, S.; Yang, L.; Liu, J. Detection and Direct Readout of Drugs in Human Urine Using Dynamic Surface-Enhanced Raman Spectroscopy and Support Vector Machines. *Anal. Chem.* **2015**, *87* (5), 2937−2944.

(55) Li, X.; Yang, T.; Li, S.; Jin, L.; Wang, D.; Guan, D.; Ding, J. Noninvasive Liver Diseases Detection Based on Serum Surface Enhanced Raman Spectroscopy and Statistical Analysis. *Opt. Express* **2015**, *23* (14), 18361−18372.

(56) Li, J.; Deng, T.-S.; Liu, X.; Dolan, J. A.; Scherer, N. F.; Nealey, P. F. Hierarchical Assembly of Plasmonic Nanoparticle Heterodimer Arrays with Tunable Sub-5 Nm Nanogaps. *Nano Lett.* **2019**, *19* (7), 4314−4320.

(57) Nam, J.-M.; Oh, J.-W.; Lee, H.; Suh, Y. D. Plasmonic Nanogap-Enhanced Raman Scattering with Nanoparticles. *Acc. Chem. Res.* **2016**, *49* (12), 2746−2755.

(58) Hamon, C.; Liz-Marzán, L. M. Hierarchical Assembly of Plasmonic Nanoparticles. *Chem. - Eur. J.* **2015**, *21* (28), 9956−9963.

(59) van Belkum, A.; Dunne, W. M. Next-Generation Antimicrobial Susceptibility Testing. *J. Clin. Microbiol.* **2013**, *51* (7), 2018−2024.

(60) Ardila, D.; Kiraly, A. P.; Bharadwaj, S.; Choi, B.; Reicher, J. J.; Peng, L.; Tse, D.; Etemadi, M.; Ye, W.; Corrado, G.; Naidich, D. P.; Shetty, S. End-to-End Lung Cancer Screening with Three-Dimensional Deep Learning on Low-Dose Chest Computed Tomography. *Nat. Med.* **2019**, *25* (6), 954−961.

(61) Rajkomar, A.; Oren, E.; Chen, K.; Dai, A. M.; Hajaj, N.; Hardt, M.; Liu, P. J.; Liu, X.; Marcus, J.; Sun, M.; Sundberg, P.; Yee, H.; Zhang, K.; Zhang, Y.; Flores, G.; Duggan, G. E.; Irvine, J.; Le, Q.; Litsch, K.; Mossin, A.; Tansuwan, J.; Wang, D.; Wexler, J.; Wilson, J.; Ludwig, D.; Volchenboum, S. L.; Chou, K.; Pearson, M.; Madabushi, S.; Shah, N. H.; Butte, A. J.; Howell, M. D.; Cui, C.; Corrado, G. S.; Dean, J. Scalable and Accurate Deep Learning with Electronic Health Records. *Npj Digit. Med.* **2018**, *1* (1), 18.

(62) Ballinger, B.; Hsieh, J.; Singh, A.; Sohoni, N.; Wang, J.; Tison, G. H.; Marcus, G. M.; Sanchez, J. M.; Maguire, C.; Olgin, J. E.; Pletcher, M. J. DeepHeart: Semi-Supervised Sequence Learning for Cardiovascular Risk Prediction. *AAAI-18: Thirty-Second AAAI Conference on Artificial Intelligence*, New Orleans, Feb 2−7, 2018.

(63) Lobritz, M. A.; Belenky, P.; Porter, C. B. M.; Gutierrez, A.; Yang, J. H.; Schwarz, E. G.; Dwyer, D. J.; Khalil, A. S.; Collins, J. J. Antibiotic Efficacy Is Linked to Bacterial Cellular Respiration. *Proc. Natl. Acad. Sci. U. S. A.* **2015**, *112* (27), 8173−8180.

(64) Guo, A. C.; Jewison, T.; Wilson, M.; Liu, Y.; Knox, C.; Djoumbou, Y.; Lo, P.; Mandal, R.; Krishnamurthy, R.; Wishart, D. S. ECMDB: The E. Coli Metabolome Database. *Nucleic Acids Res.* **2012**, *41* (D1), D625−D630.

(65) Li, J.; Xie, S.; Ahmed, S.; Wang, F.; Gu, Y.; Zhang, C.; Chai, X.; Wu, Y.; Cai, J.; Cheng, G. Antimicrobial Activity and Resistance: Influencing Factors. *Front. Pharmacol.* **2017**, *8*, 364.

(66) Zhang, R.; Xie, H.; Cai, S.; Hu, Y.; Liu, G.; Hong, W.; Tian, Z. Transfer-Learning-Based Raman Spectra Identification. *J. Raman Spectrosc.* **2020**, *51* (1), 176−186.

(67) Premasiri, W. R.; Lee, J. C.; Sauer-Budge, A.; Théberge, R.; Costello, C. E.; Ziegler, L. D. The Biochemical Origins of the Surface-Enhanced Raman Spectra of Bacteria: A Metabolomics Profiling by SERS. *Anal. Bioanal. Chem.* **2016**, *408* (17), 4631−4647.

(68) Yang, J. H.; Wright, S. N.; Hamblin, M.; McCloskey, D.; Alcantar, M. A.; Schrübbers, L.; Lopatkin, A. J.; Satish, S.; Nili, A.; Palsson, B. O.; Walker, G. C.; Collins, J. J. A White-Box Machine Learning Approach for Revealing Antibiotic Mechanisms of Action. *Cell* **2019**, *177* (6), 1649−1661.

(69) Martiny, D.; Debaugnies, F.; Gateff, D.; Gérard, M.; Aoun, M.; Martin, C.; Konopnicki, D.; Loizidou, A.; Georgala, A.; Hainaut, M.; Chantrenne, M.; Dediste, A.; Vandenberg, O.; Van Praet, S. Impact of Rapid Microbial Identification Directly from Positive Blood Cultures Using Matrix-Assisted Laser Desorption/Ionization Time-of-Flight Mass Spectrometry on Patient Management. *Clin. Microbiol. Infect.* **2013**, *19* (12), E568−581.

(70) Patel, R. MALDI-TOF MS for the Diagnosis of Infectious Diseases. *Clin. Chem.* **2015**, *61* (1), 100−111.

(71) Bos, L. D. J.; Sterk, P. J.; Schultz, M. J. Volatile Metabolites of Pathogens: A Systematic Review. *PLoS Pathog.* **2013**, *9* (5), No. e1003311.

(72) Radford, A.; Narasimhan, K.; Salimans, T.; Sutskever, I. Improving Language Understanding by Generative Pre-Training. *OpenAI report*, 2018.

(73) Kirchhoff, J.; Glaser, U.; Bohnert, J. A.; Pletz, M. W.; Popp, J.; Neugebauer, U. Simple Ciprofloxacin Resistance Test and Determination of Minimal Inhibitory Concentration within 2 h Using Raman Spectroscopy. *Anal. Chem.* **2018**, *90* (3), 1811−1818.

(74) Han, Y.-Y.; Lin, Y.-C.; Cheng, W.-C.; Lin, Y.-T.; Teng, L.-J.; Wang, J.-K.; Wang, Y.-L. Rapid Antibiotic Susceptibility Testing of Bacteria from Patients' Blood *via* Assaying Bacterial Metabolic Response with Surface-Enhanced Raman Spectroscopy. *Sci. Rep.* **2020**, *10* (1), 12538.

(75) Adams, S. M.; Campione, S.; Caldwell, J. D.; Bezares, F. J.; Culbertson, J. C.; Capolino, F.; Ragan, R. Non-Lithographic SERS Substrates: Tailoring Surface Chemistry for Au Nanoparticle Cluster Assembly. *Small* **2012**, *8* (14), 2239−2249.

(76) Bhattacharjee, A.; Nusca, T. D.; Hochbaum, A. I. Rhamnolipids Mediate an Interspecies Biofilm Dispersal Signaling Pathway. *ACS Chem. Biol.* **2016**, *11* (11), 3068−3076.

(77) Savitzky, A.; Golay, M. J. E. Smoothing and Differentiation of Data by Simplified Least Squares Procedures. *Anal. Chem.* **1964**, *36* (8), 1627−1639.

(78) Eilers, P.; Boelens, H. Baseline Correction with Asymmetric Least Squares Smoothing. *Leiden Univ. Med. Cent. Report*, 2005.

(79) Hertel, L.; Collado, J.; Sadowski, P.; Ott, J.; Baldi, P. Sherpa: Robust Hyperparameter Optimization for Machine Learning. *arXiv Preprint* **2020**, No. arXiv:2005.04048[cs.LG].

(80) Chawla, N. V.; Bowyer, K. W.; Hall, L. O.; Kegelmeyer, W. P. SMOTE: Synthetic Minority Over-Sampling Technique. *J. Artif. Intell. Res.* **2002**, *16*, 321−357.

(81) Kingma, D. P.; Welling, M. Auto-Encoding Variational Bayes. *arXiv Preprint* **2013**, No. arXiv:1312.6114[stat.ML].

(82) Liu, F. T.; Ting, K. M.; Zhou, Z. Isolation Forest. *8th IEEE Int. Conf. Data Mining* **2008**, 413−422.

(83) Roberts, S. J.; Husmeier, D.; Rezek, I.; Penny, W. Bayesian Approaches to Gaussian Mixture Modeling. *IEEE Trans. Pattern Anal. Mach. Intell.* **1998**, *20* (11), 1133−1142.